JOURNAL OF AIRCRAFT
Vol. 43, No. 5, September–October 2006

Sensitivity Study of Downwash Weighting Methods for Transonic Aeroelastic Stability Analysis

Roberto G. A. Silva,* Olympio A. F. Mello,† and João Luiz F. Azevedo‡
Instituto de Aeronáutica e Espaço, 12228-904 São José dos Campos, Brazil

DOI: 10.2514/1.16886

The paper is concerned with downwash correction methods for aeroelastic stability analyses in the transonic regime. A finite-difference Navier–Stokes code is used to calculate the unsteady aerodynamic loading due to dynamic angle-of-attack variations in three-dimensional transonic flow. The computed unsteady pressure coefficients are used as a reference state for flutter analyses using the downwash weighting method. The effects of the amplitudes of motion used in the calculation of nonlinear, unsteady reference pressures are addressed. The test case considered is the well-known AGARD wing 445.6 standard aeroelastic configuration. The configuration is subjected to rigid-body pitching oscillation about the midchord point at the root section. Flutter boundaries are computed using unsteady pressures, in the downwash correction methodology, as reference conditions to compute weighting operators. The results are compared with available experimental data and they indicate that the aerodynamic interference and viscous and thickness effects play an important role on the flutter prediction capability.

Nomenclature

a = speed of sound
b = reference length, taken as the semichord
c = chord, $2b$
C_p = pressure coefficient
$[D]$ = kernel function matrix
$[F]$ = substantial derivative operator
h = displacement mode shape vector
i = receiving point index
Im( ) = imaginary part of a complex number
inst = index indicating instantaneous quantity
j = sending point index
k = reduced frequency based on the freestream flow speed
k_r = reduced frequency based on the speed of the sound
K_ψ = kernel of the integral relation in terms of the acceleration potential
$\{L_a\}$ = aerodynamic load vector
M_∞ = freestream Mach number
n = panel number index
nl = index indicating nonlinear quantity
q = dynamic pressure
Re( ) = real part of a complex number
S = lifting surface area
$[S]$ = integration matrix
U_∞ = freestream speed
W = wake surface area
[WT] = weighting function
$\{w\}$ = downwash vector
$\{\bar{w}\}$ = nondimensional downwash vector
$\bar{x}, \bar{h}$ = planar position of doublet (discrete kernel function method)
α = angle of attack
ΔC_p = pressure difference coefficient
$\Delta\alpha$ = dynamic angle of attack
$\Delta\tau$ = nondimensional time step
ζ = coordinate in curvilinear system, aligned with the spanwise direction
η = coordinate in curvilinear system, normal to the lifting surface
ξ = coordinate in curvilinear system, tangent to the lifting surface boundary, in the streamwise direction
τ = nondimensional time
∞ = freestream condition

Presented as Paper 5375 at the 22nd Applied Aerodynamics Conference and Exhibit, Providence, RI, 17–20 August 2004; received 30 March 2005; revision received 14 December 2005; accepted for publication 18 December 2005.

*Associate Research Engineer, Head of the Aeroelasticity and Vibrations Branch, Centro Técnico Aeroespacial; rasilva@iae.cta.br.

†Senior Research Engineer. Head of the Aeronautical Systems Division, Centro Técnico Aeroespacial; oamello@iae.cta.br. Senior Member AIAA.

‡Senior Research Engineer, Head of the CFD Branch, Centro Técnico Aeroespacial; azevedo@iae.cta.br. Associate Fellow AIAA.

I. Introduction

THE most common way of performing aeroelastic analyses in the aeronautical industry is by the use of the structural-dynamic/unsteady aerodynamic commercial codes based on linear unsteady aerodynamic modeling techniques combined with structural dynamics solvers. Usually, linear aerodynamic modeling techniques are based on discrete element solutions of the linear equations of the fluid flow. However, the application of discrete element (panel) methods is limited to purely subsonic or supersonic flows, because the governing equations over which the method were developed are based on a linearized unsteady potential flow hypothesis. However, the aeroelastic behavior of an aircraft is typically critical in the transonic flight regime, where nonlinear phenomena related to embedded moving shock waves and viscosity play an important role in aeroelastic stability.

As discussed by Ashley [1], the shock wave movement and strength profoundly affect the flexure-torsion flutter mechanism. One consequence of this behavior is the so-called transonic dip phenomenon. This phenomenon is characterized by a decrease of the slope of the flutter speed plot as a function of the Mach number, when compared to the same plot obtained from a linear aeroelastic analysis. Therefore, it is necessary to pay special attention to the flutter phenomenon under these circumstances. This is especially significant as most modern aircraft fly under transonic flow conditions.

One of the feasible alternatives for analyzing the aeroelastic stability in nonlinear flow conditions is the use of time accurate computational fluid dynamic (CFD) solutions of the nonlinear fluid equations coupled with a structural-dynamic representation of the vehicle. Another approach is the use of wind tunnel testing of aeroelastic models, under transonic flow conditions. However, wind tunnel testing for aeroelastic investigation regarding flutter boundary computation is not usual because such class of experiments involves expensive models and high operational costs. In most cases of

experimental aeroelastic stability investigation, the objective is to obtain accurate measurement data to validate computational procedures applied to the solution of nonlinear equations. Examples of experiments on unsteady aerodynamics regarding pressure measurements have been reported in the literature [2–4]. Notable examples of experimental flutter investigations have been presented in [5–8]. Still another way to evaluate the transonic aeroelastic behavior is from flutter flight testing, which is the most hazardous and expensive option in terms of operational cost. This approach may be used either for experimental flutter boundaries identification or to verify the subcritical aerodynamic damping at specific flight envelope points to validate aeroelastic numerical models.

There have been several attempts to solve the transonic aeroelastic problem using combined procedures which relate linear models to measured data for the correction of unsteady linear aerodynamic models. A good review on correction techniques was presented in [9], describing the most employed methods concerning transonic flutter prediction via combined procedures. Such approaches are named here as mixed procedures. The purpose of such procedures is to correct the linear aerodynamic models to take into account nonlinear effects, unpredictable by the linearized potential-based equations of the fluid flow. The methodologies for the solution of the transonic aeroelastic problem based on mixed procedures are referred also as semiempirical corrections. These corrections can be performed by the multiplication, addition, or the whole replacement of the aerodynamic influence coefficient (AIC) matrix. This approach is an adequate tool for engineering applications, because the methodology employed is less expensive than direct use of CFD techniques.

The correction techniques, which have been applied to unsteady loading calculation for static or dynamic stability analysis, are here classified as a pressure matching method [10]. The matching of the pressures based on downwash correction consists in the modification of the control point displacement vector to satisfy a given reference pressure distribution. The advantage of pressure matching methods is related to the use of pressures instead of loads as reference conditions. The use of loads to correct an AIC matrix, which relates downwash to pressures, may lead to distortions of the pressure distributions regarding shock wave positioning and strength [10]. This problem does not happen when one uses a properly defined AIC matrix, which relates loads to the corresponding displacements in the airfoil section degrees of freedom. However, the AIC matrices, which result from the conventional modeling based on discrete element solutions of the linearized potential flow equations, relate pressures to displacements at control points. Therefore, it is natural to employ the pressure matching for the correction of the discrete element models. The nonlinear reference pressures may be computed from steady-state CFD solutions or they may be obtained from experimental measurements.

The computation of the weighting function is based on quasi-steady pressure slopes [11]. The choice of the pressure rates instead of their absolute values is made to have displacement-independent weighting functions. The next step is the definition of a prescribed quasi-steady downwash mode shape. One suggestion is the use of a pitch mode, for example. However, it is possible to employ other patterns of displacements, such as a frozen structural mode shape. The resulting weighting function will post-multiply the AIC matrix, that is, it will operate over the downwash vector. The aeroelastic analysis is performed considering such weighting operator as a post-multiplier of the AIC matrices, for all reduced frequencies to be explored in the aeroelastic study.

Generally, the pressure or load matching procedures, based on steady reference conditions, fail in obtaining unsteady pressures at higher frequencies. The magnitude of these pressures is well approximated, but the phases present wrong trends. This is so because the pressure amplitudes do not experience large variations with the reduced frequencies as it happens with the pressure phases [1]. The reason for this fact is the absence of unsteady transonic flow information in the reference conditions [1,12].

The objective of the present work is therefore, to study downwash weighting procedures applied to aeroelastic stability analysis based on nonlinear unsteady pressures as reference conditions. Such unsteady pressures are computed from unsteady CFD solutions for a prescribed motion of the lifting surface. Downwash weighting procedures are chosen due to their robustness and advantageous features such as cost and consistency with the physics of the problem [10].

II. Modeling Considerations

A. Integral Solution of the Linearized Potential Flow Equation

The aerodynamic modeling of unsteady linear potential flows is performed based on methods such as the discrete kernel function approach. The development of discrete element kernel function methods is based on integral solutions of the small disturbances linearized potential flow equation [13] for a configuration of interest. The integral solution is obtained by the application of Green's theorem to this equation [14] in terms of unsteady source and doublet singularity distributions, over the body surface S and its associated wake surfaces W.

The objective of discrete kernel function methods is to solve the problem of unsteady aerodynamic modeling of general aircraft configurations, by subdividing its surface, as well as the associated wakes, in discrete elements (panels). It is assumed that each of these elements contain elementary solutions of the governing equations. Each panel contains a control point where the boundary condition is imposed. The integral equation is approximated by the summation of elementary integrals associated with each panel. These elementary integrals at each panel, as well as the aerodynamic interference of one panel onto others, lead to a linear system of equations relating the pressure coefficient differences to downwash. The assembly of the elementary integral solutions results in a matrix which elements represent the aerodynamic influence of the panels into the control points. This matrix is named as the aerodynamic influence coefficients matrix, which relates the structural deformations to the aerodynamic forces. Each integral relationship between the downwash at a receiving point i, and the pressures at a sending panel j can be written as a system of equations as

$$\varphi_z^i = w_i = D_{ij}\Delta C_{pj} \tag{1}$$

where each of the matrix elements D_{ij} is the result of the integration of the kernel function over the given jth lifting surface element geometry [14]:

$$D_{ij} = -\frac{1}{8\pi} \times \int_{\bar{\xi}_{j-1}}^{\bar{\xi}_j} \int_{\bar{\eta}_{j-1}}^{\bar{\eta}_j} \left\{ \lim \left[\frac{\partial}{\partial z} K_\psi (x_i - \bar{\xi}_n, y_i - \bar{\eta}_n, 0, M_\infty, k) \right] \right\} \mathrm{d}\bar{\xi}_n \, \mathrm{d}\bar{\eta}_n \tag{2}$$

The inverse of the matrix operator D multiplied by the downwash vector yields the pressure distribution. In other words, the solution of the system of equations gives the doublet strength at each panel referred to a given downwash which is related to a displacement mode shape. The resulting inverse matrix is named as the aerodynamic influence coefficients matrix, which is a function of the reduced frequency, and it is related to the pressure distribution by

$$\{\Delta C_p(ik)\} = [\mathrm{AIC}(ik)]\{w(ik)\} \tag{3}$$

One should recall that a simple harmonic motion is assumed, hence the dependence on ik. The coefficients of this matrix may be interpreted as rates of pressure variation due to a given displacement amplitude input associated to the boundary conditions. Then, the determination of the pressure coefficient vector in Eq. (3) is performed from the known downwash, which is related to the amplitude of the pitch and plunge motion at each element. The substantial derivative of a given displacement mode is composed of a derivative of the normal direction displacement with respect to the main flow direction plus the associated velocity scaled by the undisturbed flow speed which, in a small disturbance sense, represents an angle of attack. Therefore, from the boundary

conditions for those small perturbations, the relationship between the normal wash and a solid boundary displacement is rewritten as

$$\{w(x,y,0,ik)\} = \frac{\partial h(x,y,0)}{\partial x} + ikh(x,y,0) = [F(ik)]\{h(x,y,0)\} \tag{4}$$

The substantial derivative applied to a given modal displacement vector $\{h\}$, which appears in Eq. (4), is denoted by the matrix operator $[F(ik)]$. The resulting aerodynamic loading vector, $\{L_a(ik)\}$, may be expressed as the multiplication of the pressures by an integration matrix $[S]$, which is constructed from the panel elements geometrical characteristics. The resulting final expression for the unsteady loading over the lifting surface is given by

$$\{L_a(ik)\} = q_\infty[S][\mathrm{AIC}(ik)][F(ik)]\{h(x,y,0)\},$$
$$\text{with } [F(ik)](\cdot) = \left[\frac{\partial(\cdot)}{\partial x} + ik(\cdot)\right] \tag{5}$$

The subsonic discrete kernel function approach will be further employed as the unsteady aerodynamic theory for computation of unsteady pressures and loads for aeroelastic response and stability analysis.

B. Aeroelastic Model

The equations of motion of a discrete aeroelastic system can be represented as an equilibrium relation between the structural and aerodynamic forces. The flutter boundary computation should be performed by solving the complex eigenvalue problem of this system, for a given parameter variation. The solution of the eigenvalue problem requires that the homogeneous aeroelastic system of equations be written into the Laplace domain.

The induced aerodynamic loading is obtained by a convolution integral which transforms the aerodynamic loading from the time domain to the Laplace domain. However, the AIC matrix is only available in the simple harmonic reduced frequency domain. Thus, it is assumed a simple harmonic motion aerodynamics, valid for stability analysis of the aeroelastic system, because damping at this condition is zero. Moreover, this hypothesis is mathematically consistent with the assumption of the simple harmonic motion introduced by the unsteady aerodynamic formulation.

The stability of an aeroelastic system is evaluated by using flutter solution techniques. These methods are based on the solution of the eigenvalue problem with respect to a given parameter variation. Some examples of flutter solutions techniques are the well-known k method due to Theodorsen [15], also presented by Rodden and Johnson [16], and Rodden and Bellinger [17]; the p–k method, Hassig [18]; and the g method [19]. The p–k method is the chosen procedure to be applied for flutter computations in the present work.

C. The Navier–Stokes Nonlinear Aerodynamic Model

The nonlinear aerodynamic computations were based in the finite difference solutions of the Navier–Stokes equations to have steady and unsteady pressures distribution over the lifting surfaces. The Navier–Stokes solver used for unsteady flow computations is a modified version of a code developed by Sankar and Kwon [20]. It is an implicit finite difference solution of the vector form of the full Reynolds-averaged, three-dimensional Navier–Stokes equations based on an arbitrary curvilinear coordinate system. All spatial derivatives are approximated by standard second-order central differences. The mathematical formulation and the description of the numerical method have been described elsewhere [21].

A slightly modified version of the Baldwin–Lomax algebraic turbulence model [22] is used, where the maximum shear stress is used instead of the wall shear stress because in the vicinity of separation points, the shear stress values approach zero at the wall. It should be noted that this change to the Baldwin–Lomax model allows the method to treat mild separation, but it is not clear to what extent the results would be valid for massive separation. Because the scope of the present investigation is the computation of unsteady flow behavior of oscillating wings at moderate amplitudes of angle of attack, this model is adequate and will be applied to the problems at hand [23].

The boundary conditions must be specified along the solid surface, at the wing root and the far field boundaries. The far field boundaries are located outboard of the wing tip, downstream beyond the trailing edge. The velocity normal to the boundary is computed. Then, the boundary conditions are imposed depending on whether it is an inflow or outflow and whether it is subsonic or supersonic.

1) Supersonic outflow: All variables are extrapolated from the interior of the domain.

2) Subsonic outflow: The pressure is fixed to be the freestream value and the other variables are extrapolated.

3) Subsonic inflow: The density is extrapolated from the interior of the domain and the other variables are fixed from the freestream.

4) Supersonic inflow: All variables are fixed to be the freestream values.

III. Downwash Correction Method

The main purpose of the correction methods to be developed here is the computation of unsteady transonic flows for dynamic aeroelastic response and aeroelastic stability analysis [10]. The main idea of such procedure is the modification of the downwash vector inside the pressure to downwash linear relationship. The transonic flow reference conditions can be based on either CFD solutions of the nonlinear fluid dynamic governing equations [20,21], or experimental data.

The basic equation over which this procedure is developed is the algebraic pressure to downwash relationship, derived from the application of discrete element kernel function methods to model the linearized potential flow equation. This relation is rewritten in a simplified form as a function only of the reduced frequency as

$$\{\Delta C_p(ik)\} = [\mathrm{AIC}(ik)]\{w(ik)\} \tag{6}$$

The downwash vector is related to the lifting surface displacements by boundary conditions defined in a small disturbances context, and may be regarded as an effective dynamic angle of attack at each of the lifting surface elements. In the frequency domain, these boundary conditions are rewritten here as

$$\{w(x,y,0,ik)\} = \frac{\partial}{\partial x}\{h(x,y,0)\} + ik\{h(x,y,0)\} \tag{7}$$

recalling that $\{h(x,y,0)\}$ is an out-of-plane lifting surface displacement mode shape, and $\{w(x,y,0.ik)\}$ is the resulting downwash with respect to the modal motion. When steady-state pressures are considered as reference conditions [10], the corresponding downwash is reduced to the derivative of the associated mode shape displacements with respect to the flow direction x as,

$$\{w(x,y,0)\} = \frac{\partial}{\partial x}\{h(x,y,0)\} \tag{8}$$

leading to a steady-state pressure to downwash relationship given by

$$\{\Delta C_p(ik=0)\} = [\mathrm{AIC}(ik=0)]\{h_x(x,y,0)\} \tag{9}$$

Another capability of downwash correction procedures is the use of computed or experimental unsteady pressure differences. In such cases, the reference conditions are based on frequency-dependent pressures, computed from the time domain aerodynamic response. Pressure time histories, for example, may result from the lifting surface displacements due to a prescribed motion. These displacements are arbitrary, as they may be, for example, impulse-type or oscillating harmonic motions. For the present downwash correction investigation, the unsteady pressure differences computation was performed based on a time domain CFD solution of the Navier–Stokes equations, using the finite differences approach mentioned in Sec. II.

The chosen displacement may be any unsteady motion associated to a displacement mode shape of the lifting surface. In the present investigations, it is chosen a rigid body harmonic pitching rotation around the root midchord axis of the lifting surface, at a preset reduced frequency k_r. This motion leads to an unsteady downwash, which also may be regarded as an unsteady perturbation in angle of attack, with amplitude equal to the amplitude of the pitching motion, $\Delta\alpha$.

Because the linear aerodynamic model to be corrected is defined in the frequency domain, it shall be necessary to transform the reference time domain pressure differences to the frequency domain. The most adequate approach is the first harmonic components computation of the pressure differences using a Fourier transform algorithm applied to their time histories. The Fourier transformations used herein to obtain the frequency domain components of the pressure differences are given by [21]

$$\begin{aligned} \mathrm{Re}\,[\Delta C_p^{\mathrm{nl}}(ik_r)] &= \frac{k}{\pi}\int_{\tau_1}^{\tau_1+2\pi/k_r} \Delta C_p(\tau)\sin(k_r\tau)\,\mathrm{d}\tau \quad \text{and} \\ \mathrm{Im}[\Delta C_p^{\mathrm{nl}}(ik_r)] &= \frac{k}{\pi}\int_{\tau_1}^{\tau_1+2\pi/k_r} \Delta C_p(\tau)\cos(k_r\tau)\,\mathrm{d}\tau \end{aligned} \tag{10}$$

where k_r is given by $k_r = \omega c/a_\infty$ and $\tau = a_\infty t/c$ is the nondimensional time, as defined in the nondimensionalization of the Navier–Stokes equations. Because the time domain simulation of the Navier–Stokes equations is based on a discrete time marching algorithm, the Fourier integrals, presented in relations (10), shall be approximated by discrete Fourier transforms as follows:

$$\begin{aligned} \mathrm{Re}\,[\Delta C_p^{\mathrm{nl}}(ik_r)] &= \frac{k_r M_\infty \Delta\tau}{2\pi\Delta\alpha}\sum_{m=m_1}^{m_1+m_T} \Delta C_{pm}\sin(k_r m\Delta\tau) \quad \text{and} \\ \mathrm{Im}[\Delta C_p^{\mathrm{nl}}(ik_r)] &= \frac{k_r M_\infty \Delta\tau}{2\pi\Delta\alpha}\sum_{m=m_1}^{m_1+m_T} \Delta C_{pm}\cos(k_r m\Delta\tau) \end{aligned} \tag{11}$$

where $\Delta\tau$ is the computational nondimensional time step over which the time marching simulation was performed. Therefore, the complex first harmonic components of the pressure coefficient differences $\Delta C_p^{\mathrm{nl}}(ik)$ are obtained from the real and imaginary part of the first harmonic components, given by Eqs. (11) as

$$\{\Delta C_p^{\mathrm{nl}}(ik_r)\} = [\mathrm{Re}\{\Delta C_p^{\mathrm{nl}}(ik_r)\}] + i[\mathrm{Im}\{\Delta C_p^{\mathrm{nl}}(ik_r)\}] \tag{12}$$

Because the unsteady pressure differences $\{\Delta C_p^{\mathrm{nl}}(ik_r)\}$ are computed, it is possible to determine correction factors, which satisfy a system of equations analogue to Eq. (9). Special care needs to be taken regarding definition of the reduced frequency for the Navier–Stokes simulations. The reduced frequency differs from that defined for the discrete element kernel function method by a factor of $k_r = k(M_\infty c/b)$, because $k = \omega b/U_\infty$. Thus, to have unsteady pressures computed by the Navier–Stokes simulation and kernel function methods at the same reduced frequency, the aforementioned relation needs to be satisfied. Another feature to be noted is that the unsteady pressure coefficients are divided by the amplitude of the motion, $\Delta\alpha$, as indicated in Eqs. (11).

The system of Eqs. (6) is now rewritten as function of a frequency-dependent weighting operator given by

$$\{\Delta C_p^{\mathrm{nl}}(ik_r)\} = [\mathrm{AIC}(ik_r)][\mathrm{WT}(ik_r)]\{\bar{w}(ik_r)\} \tag{13}$$

where $\{\bar{w}(ik_r)\}$ is the downwash vector divided by amplitude of the motion $\Delta\alpha$. The diagonal weighting matrix coefficients are obtained from the ratio between a modified unsteady downwash, computed by

$$\{w^{\mathrm{nl}}(ik_r)\} = [\mathrm{AIC}(ik_r)]^{-1}\{\Delta C_p^{\mathrm{nl}}(ik_r)\} \tag{14}$$

and the known downwash associated to the prescribed lifting surface motion, leading to

$$[\mathrm{WT}(ik_r)]_{ii} = [w^{\mathrm{nl}}(ik_r)]_i/[\bar{w}(ik_r)]_i \tag{15}$$

The nonlinear unsteady aerodynamic loading computation is performed by introducing in Eq. (5) the correcting weighting operator, which multiplies the downwash vector, leading to an approximate aerodynamic loading given by

$$\{L_a^{\mathrm{nl}}(ik_r)\} = q_\infty[S][\mathrm{AIC}(ik_r)][\mathrm{WT}(ik_r)]\{w(ik_r)\} \tag{16}$$

The choice of the reduced frequency over which the nonlinear unsteady pressure differences are referred is arbitrary; however, a good suggestion is the flutter reduced frequency predicted from the purely linear stability analysis of the aeroelastic model [10]. This assumption allows the best correction of the unsteady aerodynamic loading at the critical reduced frequency, representing an improvement on the prediction of transonic effects near the flutter boundary. However, for different reduced frequency values, there is no guarantee that the computation of the unsteady transonic loading has physical significance. This is so because the weighting function is computed based on a given reduced frequency value, which shall be different from the one in this different unsteady flow condition.

IV. Results

A. Analysis of the Unsteady Pressures for the AGARD Wing

The results to be presented in this section are obtained using downwash correction methods, based on unsteady pressures as the nonlinear reference conditions. The test case to be investigated is the AGARD wing 445.6 weakened model no. 3 [6], in subsonic to transonic flow conditions. As a first step, the unsteady pressure distribution over the AGARD 445.6 wing are investigated to understand the fluid dynamic behavior as it affects the flutter computation for this wing.

The AGARD wing 445.6 has an aspect ratio of 4.0 and a NACA 65A004 airfoil section. This wing is modeled by the doublet lattice method, implemented in MSC/NASTRAN$^{\mathrm{TM}}$ software system [24], as an isolated wing in different flow conditions, where the discrete element model is composed of 240 panels. The test conditions belong to a subset of those presented in the work of Yates [6], which consists in an experimental investigation of the aeroelastic behavior of this wing under transonic flow conditions. The model under investigation is described by Yates, regarding its structural and geometrical characteristics.

The computation of the nonlinear unsteady pressures is performed from the finite difference solution of the Navier–Stokes equations, using the method described in Sec. II. The current implementation was previously employed to the case study of the F-5 wing [10,21], which has some common aspects when compared with the case of the AGARD wing, e.g., low thickness profile, low aspect ratio, and transonic flow conditions. The computational mesh surrounding the wing is an algebraically generated, *C*-type topology, with 141 points in the ξ-direction, tangent to the lifting surface boundary, where 121 points are over the lifting surface itself. In the η-direction, normal to the wing surface, there are 41 points between the solid surface and the limit of the computational mesh. Finally, in the ζ-direction, there are 25 points aligned with the spanwise direction, where 17 points are over the lifting surface, and the remaining points are located between the wing tip and the computational domain limit.

The code used for the Navier–Stokes solution discussed in the present effort was extensively validated as demonstrated in [10,21], for the case of the F-5 wing performing harmonic oscillations. In these references, the results of the code were compared with experimental data showing good agreement in terms of unsteady pressures computations. Such calculations have considered extensive parameter variations, including several angles of attack, reduced frequencies, and amplitudes of motion. Furthermore, the calculations have also considered mesh refinement investigations to quantify the mesh effects in the Navier–Stokes solutions. Hence, because the test case considering the F-5 wing has several common aspects with the current AGARD wing test case, for instance, low thickness profile, low aspect ratio wing, and transonic flow conditions, the authors felt that they could use the experience from the work in [10,21] to reduce the number of computational runs for

Table 1 Reduced frequencies for AGARD wing 445.6 aeroelastic analysis

Mach	k_r	k
0.678	0.48839	0.36016
0.901	0.34076	0.18910
0.960	0.28252	0.14714

the present AGARD wing transonic flow investigation. Therefore, the mesh sizes for the present work were selected following the experience acquired with the F-5 study ([10,21]) and, in particular, the lessons learned in that study with regard to adequate mesh sizes for the present unsteady calculations. Hence, the meshes here used are essentially identical in size to the best compromise achieved in the F-5 study in terms of grid size, except that the current meshes have more points in the spanwise direction because the AGARD wing has a larger aspect ratio that the F-5 wing.

The investigation of the unsteady transonic flow behavior around the AGARD wing 445.6 is here performed examining pressure distributions at spanwise station 30.8%. The main concern of this investigation is to verify the influence of the amplitude of the motion on pressure distributions. Thus, this station was chosen because the flow is less subjected to three-dimensional effects as indicated by Silva et al. [25].

Three reduced frequencies are chosen from the test conditions, where each of them corresponds to a given Mach number, as presented by Yates [6]. These frequencies are presented in Table 1, where one should observe that $k = \omega b/U_\infty$, whereas $k_r = \omega c/a_\infty$. For both linear and nonlinear computations, $c = 2b = 1.0(m)$.

Pressure distributions are computed from the doublet lattice method and the unsteady Navier–Stokes simulation for the reduced frequencies and corresponding Mach numbers, presented in Table 1. In the case of the nonlinear solution, they were obtained for different amplitudes of oscillation, leading to pressure coefficient differences properly scaled by the magnitude of the disturbance. The computations were performed for different amplitudes to quantify the influence of the amplitude of the motion on the pressure ratios, and to compare these to the ones computed from the linear model.

The computed unsteady pressure distributions along the chord at spanwise station 30.8% are presented in Figs. 1a and 1b. The chosen amplitudes are 2.0 and 3.0 deg in angle-of-attack rotation around the root midchord axis. Both real and imaginary parts of these pressures are presented for the lower Mach number (0.678), the corresponding reduced frequency k given in Table 1, at these amplitudes of oscillation.

The results presented in Fig. 1 are the complex pressure distributions for a subsonic ($M_\infty = 0.678$) flow condition. For low amplitudes of motion (until $\Delta\alpha = 1.0$ deg, not shown here), there is a distinct leading edge suction peak [10]. However, examining the results presented in Fig. 1, it is possible to note that there is a deviation near the leading edge, for both real and imaginary parts of the pressures, for these larger amplitudes on motion. To further investigate this behavior, contour plots of the pressures at the maximum angles $\alpha_{\text{inst}} = 2.0$ deg and $\alpha_{\text{inst}} = 3.0$ deg are shown in Fig. 2, whereas instantaneous pressures at several angles of attack are plotted in Fig. 3 for $\Delta\alpha = 2.0$ deg and $\Delta\alpha = 3.0$ deg.

For both angles of attack, one should observe the appearance of a secondary suction peak that moves towards the trailing edge with the increase in motion amplitude. The displacement of this secondary pressure suction peak is associated to the aerodynamic lag of the flow around the finite thickness profile, computed by the Navier–Stokes solution [20].

The surface pressure distribution plots in Figs. 3a and 3b indicate that the pressure distribution is quite influenced by the motion amplitude. For example, for the same instantaneous angle of attack of 1.8 deg, it is possible to note the dependency of the aerodynamic lag on the motion amplitude. For $\Delta\alpha = 2.0$ deg (Fig. 3a), the position of the secondary pressure peak is around $x/c \cong 0.1$, whereas for $\Delta\alpha =$ 3.0 deg (Fig. 3b), the position of the secondary pressure peak is $x/c \cong 0.2$. Because these secondary pressure peaks are moving with

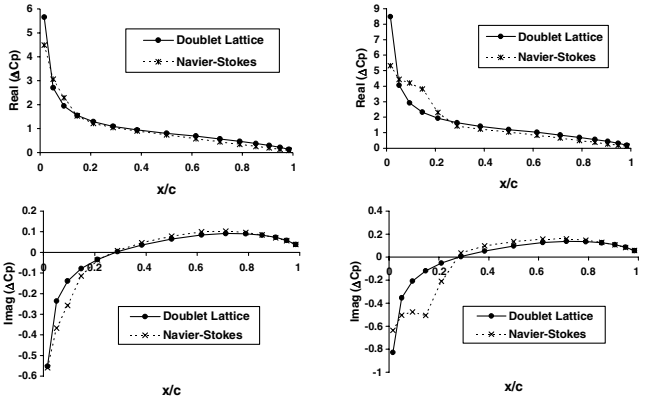

a) $\Delta\alpha = 2.0$ deg **b) $\Delta\alpha = 3.0$ deg**

Fig. 1 Unsteady pressure distributions for the wing station at 30.8% of span, $M_\infty = 0.678$.

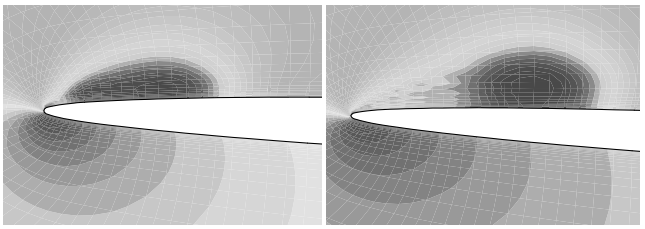

a) $\alpha_{\text{inst}} = 2.0$ deg **b) $\alpha_{\text{inst}} = 3.0$ deg**

Fig. 2 Instantaneous pressure contours at leading edge of spanwise station 30.8%, $M_\infty = 0.678$.

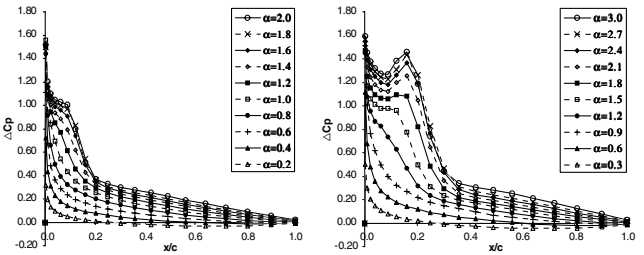

a) $\Delta\alpha = 2.0$ deg **b) $\Delta\alpha = 3.0$ deg**

Fig. 3 Instantaneous pressure distributions at spanwise station 30.8%, $M_\infty = 0.678$.

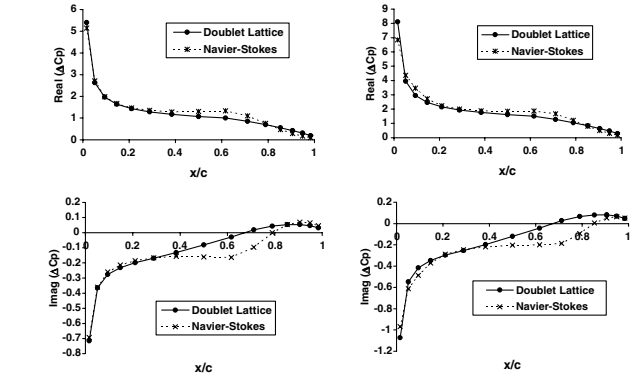

a) $\Delta\alpha = 2.0$ deg **b) $\Delta\alpha = 3.0$ deg**

Fig. 4 Unsteady pressure distributions for the wing station at 30.8% of span, $M_\infty = 0.960$.

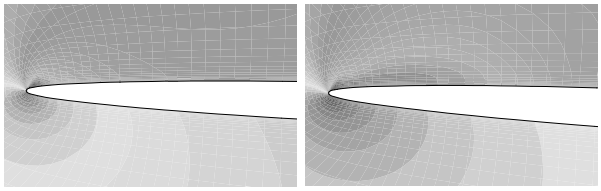

a) α_{inst} = 2.0 deg b) α_{inst} = 3.0 deg

Fig. 5 Instantaneous pressure contours at leading edge of spanwise station 30.8%, $M_\infty = 0.960$.

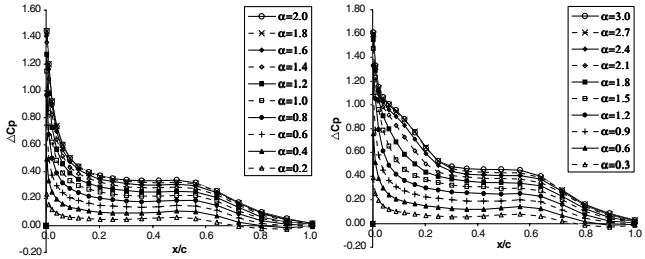

a) $\Delta\alpha$ = 2.0 deg b) $\Delta\alpha$ = 3.0 deg

Fig. 6 Instantaneous pressure distributions at spanwise station 30.8%, $M_\infty = 0.960$.

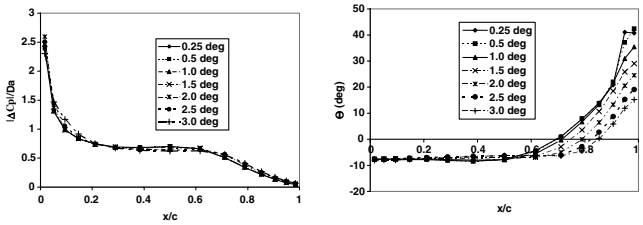

Fig. 7 Pressure difference distributions for spanwise station 30.8%, $M_\infty = 0.96$.

time, and their displacements increase with the amplitude of the motion, then the deviation from the linear complex pressure distributions are larger for the higher angle-of-attack amplitudes (Figs. 1a and 1b). The downstream displacement of the secondary pressure peak is more pronounced in the subsonic Mach number because, under this condition, the aerodynamic lag effects are more relevant.

The differences that have been observed between the doublet lattice method and the Navier–Stokes results at $M_\infty = 0.96$ (Fig. 4) are associated to a shock wave formation. Contour plots of the instantaneous pressures at maximum angle-of-attack situations are presented in Fig. 5 whereas instantaneous pressure distributions at several angles are shown in Fig. 6 for this Mach number. For $\Delta\alpha = 3.0$ deg, there is only a slight trend for appearance of a secondary peak (Fig. 6b), because the aerodynamic lag is suppressed by the high undisturbed flow speed energy.

One should observe in Figs. 6a and 6b that there is a displacement of the shock wave towards the trailing edge, from $x/c \cong 0.50$ to $x/c \cong 0.57$ for the angles of attack $\alpha = 2.0$ deg and $\alpha = 3.0$ deg, respectively. The transonic effects are more pronounced for this Mach number, and are especially evident in the imaginary part of the pressures, leading to strong differences between the linear and nonlinear predicted phases. As the pressure phases are more sensitive to the shock movement than the pressure amplitudes, the main differences when comparing the potential and the Navier–Stokes results will be in the imaginary part of the pressure.

Another feature to be noted is the influence of the amplitude of the motion on the shock wave position. In Figs. 4a and 4b, one may notice that the shock appears to move aft as the amplitude is increased. The reason for this behavior is that, in steady flow conditions, the shock wave position moves towards the trailing edge as the angle of attack is increased, as shown by Silva et al. [25]. This behavior is also noted for unsteady flows, as indicated by Dowell et al. [26]. Recalling that the pressures are scaled by the amplitude of the motion, one should note that, for smaller angles of attack, the shock position is about the same. This is so because in the low angle-of-attack range the transonic flow behaves linearly, with respect to angle of attack, as concluded by Silva [10].

The behavior of the phase angles of the scaled complex pressure difference along the chord for $M_\infty = 0.96$ is summarized in Fig. 7, where Θ is the nondimensional phase angle resulting from the scaling of the phase angle θ, computed from $\theta = \tan^{-1}[\mathrm{Im}(C_p)/\mathrm{Re}(C_p)]$, and the amplitude $\Delta\alpha$, as $\Theta = \theta/\Delta\alpha$.

As may be observed in Fig. 7, for this specific case, i.e., $M_\infty = 0.96$ and 30.8% spanwise station, pressure phases remain around -8 deg up to $x/c \cong 0.55$. Aft of that location, the pressure phase advances as the trailing edge is approached. The corresponding pressure difference amplitudes, scaled by the amplitude of the motion, are summarized in the same figure. It may be noticed that the scaled pressure difference amplitude changes only slightly as the angle-of-attack amplitude is increased.

The pressure distribution behavior, summarized in the results of this section, suggests that the amplitude of the motion plays an important role in the computation of the complex unsteady pressure distributions. The amplitude of the pressures gives the lift, whereas the pressure phases may be understood as a form to quantify the lag between the center of pressure displacement and the lifting surface motion. Because the center of pressure position is governed by the shock displacement, as indicated by Ashley [1], the moment coefficient derivatives will be more sensitive to the nonlinearities of the flow over the lifting surface. Therefore, from these observations it is suggested that the influence of the nonlinearities will promote significant changes in the computation of the aeroelastic stability, because flutter depends on the relative position of the center of pressure with respect to the elastic axis position. In the next subsection an investigation of the aeroelastic stability behavior will be performed to evaluate the influence of the amplitude of the angle of attack on the computation of flutter speeds based on nonlinear unsteady pressures.

B. AGARD 445.6 Wing Aeroelastic Stability Analysis

The computation of the aeroelastic stability of the AGARD wing is performed using either nonlinear steady [10] or unsteady pressure distribution as reference conditions. The unsteady aerodynamic modeling is based on the doublet lattice method, implemented in the MSC/NASTRAN^{TM} software system [24]. The chosen flutter solution technique is the p–k method, which is mathematically consistent for the computation of the flutter boundary. The weighting operators are computed to correct the pressure to downwash relation, resulting from the modeling of the AGARD 445.6 wing using the doublet lattice method.

The nonlinear pressures were obtained under unsteady motion to provide the corresponding reference conditions for the unsteady downwash weighting method. In this case, the pressures were computed under harmonic motion oscillations of the wing with amplitude $\Delta\alpha = 2.0$ deg, where the nonlinear contribution due to unsteady transonic effects are more relevant. In the case of the application of the downwash correction method based on steady pressures as reference conditions [10], the chosen amplitude of the quasi-steady motion is $\Delta\alpha = 0.5$ deg because the nonlinear contribution comes from the steady mean transonic flow. Indeed, this amplitude is sufficient because it will be computed quasi-steady pressure rates, which would be independent of the amplitude of the motion. Furthermore, it was identified by Silva et al. [25] that for small angles of attack (up to 2.0 deg), the flow behaves linearly with the variation in angle of attack with regard to the shock wave displacement in steady flow conditions. However, for larger angles of attack it is possible to have shock-induced separations, which are not desirable for the computation of the quasi-steady reference pressure, because this phenomenon is out of the scope of the present

Table 2 Flutter speeds and frequencies for AGARD wing 445.6

M_∞	Experimental		Linear		Steady correction		Unsteady correction	
	V_F, m/s	ω_F, Hz	V_F, m/s	ω_F, Hz	V_F, m/s	ω_F, Hz	V_F, m/s	ω_F, Hz
0.678	231.37	17.98	239.89	20.18	213.82	21.25	239.30	23.76
0.901	296.69	16.09	299.30	16.38	275.65	17.35	284.76	17.12
0.960	309.01	13.89	329.18	14.57	315.97	15.65	298.63	15.41

Table 3 Flutter speeds and frequencies for AGARD wing 445.6

M_∞	Unsteady Correction		CAP-TSD (nonlinear) (Bennet et al. [28])		ZTAIC (Chen et al. [27])	
	V_F, m/s	ω_F, Hz	V_F, m/s	ω_F, Hz	V_F, m/s	ω_F, Hz
0.678	239.30	23.76	234.09	19.2	231.95	19.30
0.901	284.76	17.12	290.17	15.8	294.19	16.38
0.95	N/A	N/A	291.39	12.8	287.91	13.46
0.96	298.63	15.41	N/A	N/A	N/A	N/A

investigation. The main concern is to have a nonlinear steady mean flow distribution with regard to the shock positioning and strength.

The weighting operators are introduced in the aeroelastic analysis as correction factors, yielding the computed flutter speeds shown in Tables 2 and 3. Table 2 presents a comparison between the transonic flutter computation based on the correction using steady and unsteady nonlinear pressures and experimental results [6]. Table 3 includes comparisons with some well-known aeroelastic analysis codes [27–29] with unsteady downwash correction procedure results.

The ZTAIC method [27] is a modal aerodynamic influence coefficient matrix correction method, based on the transonic equivalent strip method developed by Liu et al. [12] and further extended by Chen et al. [27]. The CAP-TSD method is a time domain finite difference solution of the transonic small disturbance equation [29] coupled with a finite element structural-dynamic model. The results shown in Tables 2 and 3 are also represented in graphical form in Figs. 8 and 9, respectively, in terms of the flutter speed index (FSI) as a function of the Mach number.

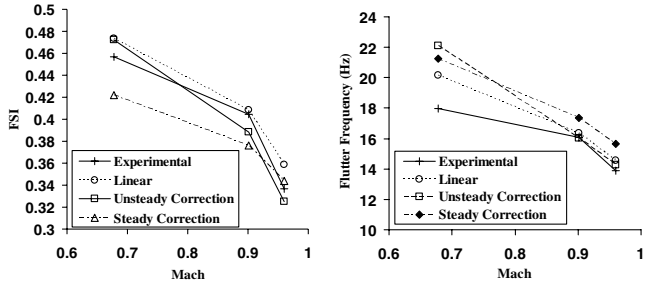

Fig. 8 AGARD wing 445.6 results: comparison of steady and unsteady downwash weighting methods.

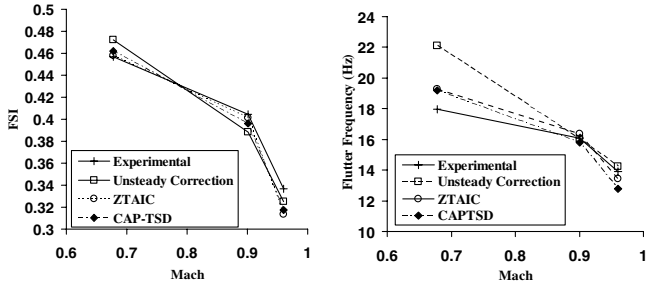

Fig. 9 AGARD wing 445.6 results: comparison of downwash weighting method and other methods.

The flutter speed index is a nondimensional flutter speed defined as $\mathrm{FSI} = V_f/(b_s\omega_\alpha\sqrt{\bar{\mu}})$, where V_f is the dimensional flutter speed, b_s is the root semichord length, and ω_α is a reference frequency. The term inside the square root is the mass ratio defined as [6] $\bar{\mu} = \bar{m}/\rho\vartheta$, where $\bar{m}$ is the mass of the wing, ρ is the flow density if the test medium, and ϑ is the volume of a conical frustum having streamwise root chord as a lower base diameter, streamwise tip as the upper base diameter, and the wing span as height. The flutter speed index computation is performed for each Mach number, depending on the freestream properties and geometrical properties of the wing, as $\mathrm{FSI}^{M_\infty=0.678} = V_f/506.7$, $\mathrm{FSI}^{M_\infty=0.901} = V_f/733.1$, and $\mathrm{FSI}^{M_\infty=0.960} = V_f/918.3$, where the flutter speed is given in SI units (m/s).

One can observe in Fig. 8 that the flutter speed indexes computed from the correction based on unsteady pressures indicate the presence of the transonic dip. This phenomenon is characterized by a decrease of the slope of the flutter speed plot as a function of the Mach number, when comparing with the linearly predicted one. In the same figure are also shown results from the correction based on steady pressures. One may notice that there is a good agreement when comparing the dip slope between the unsteady pressures based correction procedure and the experimental data. The steady pressures based correction underestimates some of the flutter speeds, as well as the dip slope. The reason for these discrepancies is related to the absence of a nonlinear unsteady pressures contribution, because the reference pressures, over which the correction factors are computed, are from steady nature.

One feature to be noted in the same results (Fig. 8) is that in the subsonic Mach number case ($M_\infty = 0.678$), the correction based on unsteady pressures did not change significantly the linear prediction. This fact can be understood by resorting to Figs. 1 and 4, where one should observe the differences in the pressure phases from the linear and nonlinear calculations, for each Mach number and for the same amplitude of the motion $\Delta\alpha = 2.0$ deg. Considering those differences between the linear and nonlinear pressure distributions, the resulting correction factors for the transonic flow conditions will properly introduce the necessary changes in the downwash vector to take into account the nonlinear behavior. However, at the subsonic flow condition the differences between the amplitude of the linear and the nonlinear computed pressures are very small and not sufficient to introduce changes in the computation of the corrected flutter speed. The same behavior is observed in the frequency plots shown in Fig. 8. Note that at $M_\infty = 0.678$ the flutter frequency is not subjected to significant changes, when comparing it with the uncorrected results. On the other hand, in the case of the computed flutter frequencies at $M_\infty = 0.901$, and $M_\infty = 0.96$, the frequencies are subjected to important changes resulting in corrected values which are in better agreement with the experimental ones.

The results presented by Chen et al. [27], as shown in Fig. 9, indicate that the transonic dip phenomenon is well characterized in

Table 4 Flutter speeds and frequencies for AGARD wing 445.6 until $\Delta\alpha = 15$ deg

M_∞	$\Delta\alpha = 0.25$ deg		$\Delta\alpha = 0.5$ deg		$\Delta\alpha = 1.0$ deg		$\Delta\alpha = 1.5$ deg	
	V_F, ft/s	ω_F, Hz	V_F, ft/s	ω_F, Hz	V_F, ft/s	ω_F, Hz	V_F, ft/s	ω_F, Hz
0.678	776.86	23.49	777.62	23.52	772.97	23.39	774.67	23.44
0.901	954.32	17.26	945.92	17.96	934.21	16.71	929.16	16.93
0.960	1046.1	15.36	1039.9	15.19	1020.5	15.47	999.35	15.26

Table 5 Flutter speeds and frequencies for AGARD wing 445.6, until $\Delta\alpha = 3.0$ deg

M_∞	Uncorrected		$\Delta\alpha = 2.0$ deg		$\Delta\alpha = 2.5$ deg		$\Delta\alpha = 3.0$ deg		Experimental	
	V_F, ft/s	ω_F, Hz	V_F, ft/s	ω_F, Hz	V_F, ft/s	ω_F, Hz	V_F, ft/s	ω_F, Hz	V_F, ft/s	ω_F, Hz
0.678	787.03	17.54	785.09	23.76	818.58	20.97	861.69	28.93	759.1	17.98
0.901	981.95	15.28	934.24	17.12	983.37	17.01	1086.22	18.03	973.4	16.09
0.960	1080.0	14.35	979.72	15.41	1021.1	15.77	1167.15	17.17	1013.8	13.89

the solution with the ZTAIC method [29], and the computed flutter speed also presents good agreement with the experimental data. The ZTAIC procedure [27] is based in a more comprehensive theory of AIC matrix correction. That method employs two-dimensional finite differences solutions for the computation of three-dimensional nonlinear unsteady pressures distributions, for a set of different downwash modes, by the use of the transonic equivalent strip method [12]. If one considers that the downwash correction method is based on unsteady pressures computed for a single pitch mode, it is clear that one should expect the ZTAIC method to yield a better correlation with the experimental data. In Fig. 9, the CAP-TSD code calculations [28] also yield good results, because its formulation is based on a finite difference nonlinear solution of the three-dimensional form of the transonic small disturbance equations. Furthermore, the ZTAIC and CAP-TSD methods represent adequately the severity in the flutter dip phenomenon, which in this case is a desirable feature in transonic flutter prediction. A disadvantage regarding such procedures is the dependency on two- and three-dimensional unsteady finite difference solutions of the nonlinear equations, respectively, increasing the computational cost in comparison with the downwash correction method.

The next step is to perform a sensitivity analysis with regard to the variation of the dynamic amplitude input, which is used to generate the nonlinear unsteady pressure distribution, taken as reference conditions for the computation of the correction factors. The objective is to understand the sensitivity of the computed aeroelastic system stability margins with respect to the amplitude of the motion, which may be related to the linear/nonlinear behavior. Tables 4 and 5 present the computed flutter speeds, based on the unsteady downwash correction method, using the resulting pressures with respect to a set of displacement amplitudes.

Tables 4 and 5 include comparisons with the results computed from the uncorrected aeroelastic model and experimental measurements [6]. One should observe that the flutter speeds present significant variation with the nature of the unsteady pressure data used to compute the correction factors. These results are graphically represented in Fig. 10, as the variation of the nondimensional flutter speed (FSI) with the freestream Mach number.

In Fig. 10, it is possible to notice that the behavior of the nondimensional flutter speed with the Mach number presents a certain proportionality in the slopes of the curves up to $\Delta\alpha = 1.0$ deg. As the motion amplitude approaches this value, the predicted flutter speed for $M_\infty = 0.96$ approaches the corresponding experimental value. However, the transonic dip, which is characterized as the slope of the nondimensional flutter speed curve as a function of the Mach number, is less pronounced than the experimental one. Also in Fig. 10, another set of computed

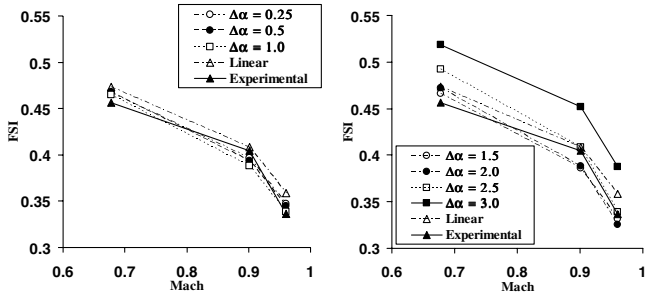

Fig. 10 Comparison between flutter speed plots as function of the amplitude of motion.

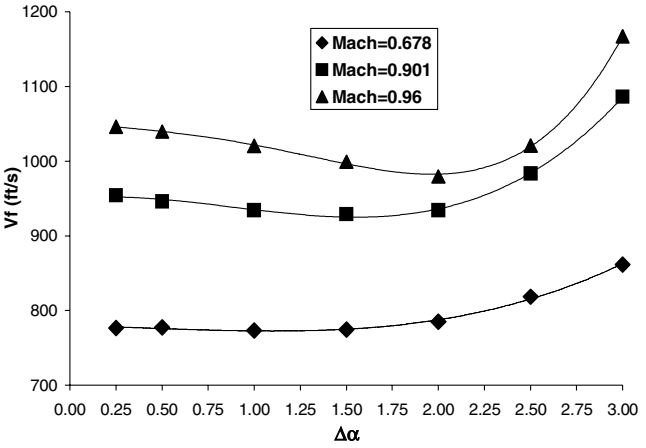

Fig. 11 Flutter speed behavior as a function of the amplitude of the motion.

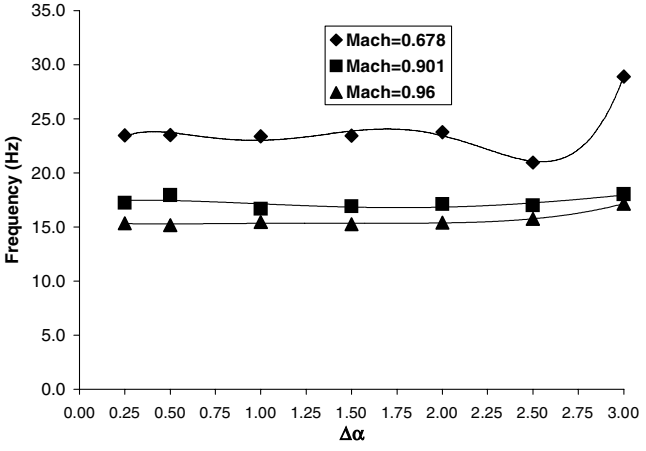

Fig. 12 Flutter frequency behavior as a function of the amplitude of the motion.

flutter speeds is presented for greater amplitudes of the dynamic angle of attack. The best results in approaching the transonic dip slope are when one considers a dynamic angle amplitude of $\Delta\alpha = 2.0$ deg, at the same time as the flutter speeds are slightly underestimated. Above this value, an interesting result should be noted. The computed flutter speeds at 2.5 deg are nearly coincident with the experimental ones in the transonic Mach number range. Otherwise, it is possible to note an increase of the flutter speeds computed at 3.0 deg. In Figs. 11 and 12 the behavior of the aeroelastic stability of the AGARD 445.6 wing is summarized graphically representing the flutter speeds and frequencies as functions of the amplitude of the motion.

It should be noted that up to $\Delta\alpha = 2.0$ deg, the flutter speed decreases, and also the transonic dip is more evident, reinforcing the fact that the transonic dip phenomenon is mainly governed by the nonlinear unsteady flow conditions. However, as soon as the angle of attack increases beyond 2.0 deg, it should be noted that the flutter speed increases with the amplitude of the motion. One possible reason for this behavior may be related to the differences in the complex pressures which may be observed in the pressure plots for the amplitudes 2.0 and 3.0 deg, given in Figs. 1a and 1b, at subsonic conditions.

Looking at these plots, one may notice that there are significant differences between the linear and the nonlinear pressures, with regard to the prediction of the leading-edge suction peak. These differences are resulting from the increase aerodynamic lag associated to the displacement of a secondary pressure peak present due to the thickness of the profile, as it was identified in Figs. 2 and 3. Thus, the center of pressure position is changed in such way that it modifies the moment on the wing. Consequently, its flutter characteristics will be a function of the amplitudes of the motion, as one should observe in Fig. 11 and 12, confirming that the aerodynamic lag effect is playing an important role in the stability of the aeroelastic system. Furthermore, it is possible to note that, up to the amplitude of 2.0 deg, the transonic dip is more evident as the angle of attack increases, indicating the nonlinearity of such phenomenon, with regard to the aerodynamic lag due to the thickness effect.

The present investigation indicates that computed flutter speeds using unsteady downwash correction method depend on amplitudes of the motion. In the linear/nonlinear investigations presented by Silva et al. [30], the transonic flow linear behavior limit could be established for disturbances in angle of attack below 0.35 deg, assuming the moment coefficient criterion. One should recall that moments play an important role in the flutter phenomenon. Therefore, the variation of the flutter speeds and frequencies as a function of amplitudes of the motion results from the nonlinear flow behavior, regarding thickness effects.

The downwash weighing method based on unsteady reference pressures requires time-accurate CFD simulations. The unsteady flow Navier–Stokes solution uses approximately 8.2 CPU hours for the simulation of two cycles of pitching motion of the AGARD 445.6 wing, in a Silicon Graphics^{TM} Octane II workstation, with two R12000 RISC architecture processors, for the meshes here employed. When the flutter analysis computational time is included, which never exceeds 5 min, the total elapsed time should be approximately 8.5 h. Such computational times are much smaller than those that would be required for a full Navier–Stokes time domain aeroelastic solution, which could involve several unsteady (aeroelastic) calculations for each flight condition.

V. Conclusion

A study on correction methods for aeroelastic stability analysis in transonic flow has been developed. Downwash correction methods for transonic flutter computation were evaluated, including a sensitivity analysis of the computed transonic flutter speeds as a function of unsteady reference pressures resulting from different amplitudes of the lifting surface motion. The conclusions that can be drawn from the present investigation are outlined in the forthcoming paragraphs.

Downwash weighting methods, using either steady [10] or unsteady pressures as reference conditions, were investigated. The transonic dip was captured with application of both correction approaches. However, the decrease of the flutter speed curve slope was more evident and closer to experiments when the unsteady downwash correction method was employed. The flutter speed curve slope obtained by the steady downwash weighting method was about the same as the one obtained by the uncorrected aeroelastic stability analysis. It may be concluded that the unsteady flow contribution, embedded in the unsteady reference pressures, plays an important role in the transonic flutter phenomenon. Furthermore, the results obtained for fully subsonic Mach numbers is justified by the good agreement between the linear and nonlinear flow solutions around the AGARD 445.6 wing. When the nonlinear solution, which is the reference condition for the construction of the downwash weighting operator, approaches the linear solution, the effect of the correction operator weighting is minimized.

The unsteady downwash weighting method requires unsteady CFD computations, increasing its cost with respect to the steady downwash weighting procedure. Furthermore, in a strict sense, it should be applied only at the specific reduced frequency for which the unsteady pressures were obtained. However, this is not a serious limitation because this reduced frequency can always be estimated from a purely linear aeroelastic analysis for the flight condition of interest. Moreover, the unsteady downwash weighting method depends on the nature of the unsteady reference pressures. In this context, a sensitivity analysis was performed to investigate the role of the unsteady reference pressure disturbances, which are referred to a given amplitude of the lifting surface motion, on the prediction of the transonic flutter. This investigation indicated that the flutter boundaries computed by unsteady downwash correction methods are significantly dependent on the unsteady pressures taken as reference conditions.

The preceding comments are consistent with the observations regarding the linear/nonlinear investigations, where it was found that the linear limit associated to the lifting moment is more sensitive to the amplitude of the motion [30]. The flutter instability is mainly governed by the lifting moment, which is associated to the streamwise displacement of the center of pressure. Detailed analyses of the local 2-D flow at several spanwise stations over the AGARD 445.6 wing indicated that there is a formation of a secondary suction peak. The displacement of this secondary suction peak may alter the position of the center of pressure. The appearance of this secondary suction peak results from the Navier–Stokes computation of the flow around the leading edge of a profile with finite thickness. Therefore, aerodynamic lag appears, which is dependent on the amplitude of the motion at a given reduced frequency. These observations explain the dependence of the computed flutter speed on these amplitudes. The overall results confirm that the nonlinear effects associated to the profile thickness play an important role in flutter prediction by correction methods based on nonlinear unsteady pressure distributions.

Acknowledgments

The second and third authors were supported by the Conselho Nacional de Desenvolvimento Científico e Tecnológico (CNPq), Brazil, under the Integrated Project Research Grant No. 501200/2003-7. The second author thanks the Fundação de Amparo à Pesquisa do Estado de São Paulo (FAPESP) for support under Grant No. 04/05188-9. Support for this research was also provided by FAPESP under Grant No. 00/13768-4.

References

[1] Ashley, H., "Role of Shocks in the 'Sub-Transonic' Flutter Phenomenon," *Journal of Aircraft*, Vol. 17, No. 3, March 1980, pp. 187–197.

[2] Lessing, H. C., Troutman, J. L., and Menees, G. P., "Experimental Determination on a Rectangular Wing Oscillating in the First Bending Mode for Mach Numbers from 0.24 to 1.30," NASA TND-33, Dec. 1960.

[3] Tijdeman, H., van Nunen, J. W. G., Kraan, A. N., Persoon, A. J., Poestkoke, R., Roos, R., Schippers, P., and Siebert, C. M., "Transonic Wind Tunnel Tests on an Oscillating Wing with External Stores, Part 2: Clean Wing," Air Force Flight Dynamics Laboratory Rept. AFFDL-TR-78-194, Pt. 2, Wright–Patterson AFB, OH, 1979 (Also Rept. NLR-TR-78106U, Pt. 2).

[4] Malone, J. B., and Ruo, S. Y., "LANN Wing Test Program: Acquisition and Application of Unsteady Transonic Data for Evaluation of Three-Dimensional Computational Methods," Air Force Flight Dynamics Laboratory Rept. AFWAL-TR-83-3006, Wright–Patterson AFB, OH, Feb. 1983.

[5] Isogai, K., "Numerical Simulation of Transonic Flutter of a High-Aspect-Ratio Transport Wing," National Aerospace Laboratory, Rept. TR-776T, Japan, Aug. 1983.

[6] Yates, E. C., Jr., "AGARD Standard Aeroelastic Configurations for Dynamic Response I-Wing 445.6," AGARD Rept. No. 765, 1988.

[7] Farmer, M. G., and Rivera, J. A., "Experimental Flutter results of a Cambered Supercritical Wing on a Pitch and Plunge Apparatus," presented at Aerospace Flutter and Dynamics Council Meeting, NASA Langley Research Center, May, 1988.

[8] Hong, M. S., Bhatia, K. G., SenGupta, G., Kim, T., Kuruvila, G., Silva, W. A., Bartels, R., and Biedron, R., "Simulations of a Twin-Engine Transport Flutter Model in the Transonic Dynamics Tunnel," Paper No. US-44, *Proceedings of the International Forum on Aeroelasticity and Structural Dynamics*, Confederation of European Aerospace Societies (CEAS), Amsterdam, June 2003.

[9] Palacios, R., Climent, H., Karlsson, A., and Winzell, B., "Assessment of Strategies for Correcting Linear Unsteady Aerodynamics Using CFD or Test Results," *Proceedings of the CEAS/AIAA International Forum on Aeroelasticity and Structural Dynamics*, Confederation of European Aerospace Societies (CEAS), Madrid, June 2001, pp. 195–210.

[10] Silva, R. G. A., "A Study on Correction Methods for Aeroelastic Analysis in Transonic Flow," Doctorate Dissertation, Aeronautics Dept., Technological Institute of Aeronautics (ITA), São José dos Campos, Brazil, 2004.

[11] Silva, R. G. A., Mello, O. A. F., and Azevedo, J. L. F., "Transonic Flutter Calculations Based on Assumed Mode Shapes Corrections," *Proceedings of the CEAS/AIAA International Forum on Aeroelasticity and Structural Dynamics*, Confederation of European Aerospace Societies (CEAS), Madrid, 2001, pp. 183–194.

[12] Liu, D. D., Kao, Y. F., and Fung, K. Y., "An Efficient Method for Computing Unsteady Transonic Aerodynamics of Swept Wings with Control Surfaces," *Journal of Aircraft*, Vol. 25, No. 1, Jan.–Feb. 1988, pp. 25–31.

[13] Landahl, M. T., *Unsteady Transonic Flow*, Pergamon, New York, 1951.

[14] Chen, P. C., Lee, H. W., and Liu, D. D., "Unsteady Subsonic Aerodynamics for Bodies and Wings with External Stores Including Wake Effect," *Journal of Aircraft*, Vol. 30, No. 5, Sep.–Oct. 1993, pp. 618–628.

[15] Theodorsen, T., "General Theory of Aerodynamic Instability and the Mechanism of Flutter," NACA Rept. No. 496, 1940.

[16] Rodden, W. P., and Johnson, E. H., "MSC/NASTRAN Aeroelastic Analysis—User's Guide Version 68," MacNeal–Schwendler Corporation, Los Angeles, 1994.

[17] Rodden, W. P., and Bellinger, E. D., "Unrestrained Aeroelastic Divergence in a Dynamic Stability Analysis," *Journal of Aircraft*, Vol. 19, No. 9, Sept. 1982, pp. 796–797.

[18] Hassig, H. J., "An Approximate True Damping Solution of the Flutter Equation By Determinant Iteration," *Journal of Aircraft*, Vol. 8, No. 11, Nov. 1971, pp. 885–889.

[19] Chen, P. C., "Damping Perturbation Method for Flutter Solution: The G-Method," *AIAA Journal*, Vol. 38, No. 9, Sept. 2000, pp. 1519–1524.

[20] Sankar, L. N., and Kwon, O. J., "High-Alpha Simulation of Fighter Aircraft," *Proceedings of the NASA High Angle-of-Attack Technology Conference*, Vol. 1, Pt. 2, NASA Langley Research Center, Hampton, VA, 1990, pp. 689–702; also NASA CP-3149.

[21] Mello, O. A. F., "An Improved Hybrid Navier-Stokes/Full-Potential Method for Computation of Unsteady Compressible Viscous flows," Ph.D. Thesis, Georgia Institute of Technology, Nov. 1994.

[22] Baldwin, B., and Lomax, H., "Thin Layer Approximation and Algebraic Model for Separated Turbulent Flows," AIAA Paper 78-257, Jan. 1978.

[23] Mello, O. A. F., and Azevedo, J. L. F., "Simulation of High Angle-of-Attack Flow over a Hemisphere-Cylinder," *Proceedings of the 8th Brazilian Congress of Engineering and Thermal Sciences, ENCIT 2000*, ABCM, Porto Alegre, Rio Grande do Sul, Brazil, 2000.

[24] MSC/NASTRAN, Software Package, Ver. 68.2, MacNeal–Schwendler Corporation, Los Angeles, 1995.

[25] Silva, R. G. A., Mello, O. A. F., and Azevedo, J. L. F., "A Numerical Study into Shock Displacement Effects for Aeroelastic Analysis in Transonic Flow," *Proceedings of the 9th Brazilian Congress of Thermal Engineering and Sciences, ENCIT 2002*, ABCM, So Jos dos Campos, Brazil, Oct. 2002.

[26] Dowell, E. H., Williams, M. H., and Bland, S. R., "Linear/Nonlinear Behavior in Unsteady Transonic Aerodynamics," *AIAA Journal*, Vol. 21, No. 1, Jan. 1983, pp. 38–46.

[27] Chen, P. C., Sarhaddi, D., and Liu, D. D., "Transonic Aerodynamic Influence Coefficient Approach for Aeroelastic and MDO Applications," *Journal of Aircraft*, Vol. 37, No. 1, Jan.–Feb. 2000, pp. 85–94.

[28] Bennet, R. M., Batina, J. T., and Cunningham, H. J., "Wing Flutter Calculations with the CAP-TSD Unsteady Transonic Small-Disturbance Program," *Journal of Aircraft*, Vol. 26, No. 9, Sept. 1989, pp. 876–882.

[29] ZAERO, Software Package, Ver. 6.5, Zona Technology, Scottsdale, AZ, 2003.

[30] Silva, R. G. A., Mello, O. A. F., and Azevedo, J. L. F., "A Navier-Stokes Based Study into Linearity in Transonic Flow fort Flutter Analysis," AIAA Paper 2002-2971, June 2002.